Applied Catalysis B: Environmental 148–149 (2014) 295–303

Contents lists available at ScienceDirect

Applied Catalysis B: Environmental

journal homepage: www.elsevier.com/locate/apcatb

A comparative study on catalytic properties of solid acid catalysts for glycerol acetylation at low temperatures

Inbae Kim, Jaesung Kim, Doohwan Lee*

Catalysis and Nanomaterials Lab, Department of Chemical Engineering, University of Seoul, Siripdae-gil 13, Jeonnong-dong, Seoul 130-743, Republic of Korea

ARTICLE INFO

Article history:
Received 25 June 2013
Received in revised form 4 November 2013
Accepted 7 November 2013
Available online 15 November 2013

Keywords:
Glycerol
Acetylation
Heterogeneous catalysts
Sulfonic acids
Fuel additives

ABSTRACT

The catalytic properties of various types of solid acids, including silica–alumina, HUSY, dodecamolybdophosphoric acids supported on Nb_2O_5 (HPMo/Nb_2O_5) and mesoporous SBA-15 (HPMo/SBA-15), Amberlyst-15, sulfated ceria–zirconia (SCZ), propylsulfonic acid functionalized SBA-15 ($PrSO_3H$-SBA-15), and sulfonic acid functionalized SBA-15 (SO_3H-SBA-15) and microcrystalline cellulose (SO_3H-Cell) catalysts, are studied for glycerol acetylation with acetic acid at low temperatures. Compared at the same acidity loading and similar glycerol conversion level (~30%) below the equilibrium, the glycerol conversion turnover rate toward di- and triacetin is considerably higher on $PrSO_3H$-SBA-15 and Amberlyst-15, with the rates shown in order as follows: $PrSO_3H$-SBA-15 > Amberlyst-15 > HPMo/Nb_2O_5 ≥ HPMo/SBA-15 > HUSY > SCZ > SiO_2–Al_2O_3. The catalytic properties of these solid acids are relatively stable under consecutive batch runs at 353 K, whereas SO_3H-SBA-15 and SO_3H-Cell deactivate with a significant acidity loss due to hydrolysis of the grafted sulfonic acid groups. When similar type of the solid acids is compared, the acid strength affect the rate and selectivity, favoring a higher acid strength for the facilitation of the reactions ($PrSO_3H$-SBA-15 > Amberlyst-15; HUSY > SiO_2-Al_2O_3; HPMo/Nb_2O_5 ≥ HPMo/SBA-15). However, the proportional correlation between the acid strength and the glycerol conversion turnover rate does not hold when different types of solid acids are compared. The orders of magnitude higher glycerol conversion turnover rates with moderate Brönsted acid strength on the sulfonic acid functionalized catalysts suggest that the configuration of surface acid moieties attribute substantially to their catalytic activity for the reactions. The acid strength on SCZ is the highest, reflecting the super acidic nature of the sites formed on the sulfated metal oxide surface, but its catalytic activity for the reactions is inferior. The glycerol conversion turnover rates on the catalysts follow the Arrhenius type temperature dependence, and the characterization results indicate that the internal mass transfer resistance does not limit the reactions.

1. Introduction

Glycerol is a byproduct of biodiesel synthesis that forms via the transesterification of natural oils, usually with C_1–C_4 alcohols [1]. The increasing biodiesel production in recent years has resulted in excess production of the glycerol byproduct (stoichiometrically 10 wt% in a biodiesel production basis), but the current market does not cope with the purification cost of crude glycerol for conventional utilizations such as in food additives, cosmetics, and surfactants [2]. The transformation of bio-glycerol into glycerol-ethers and glycerol-esters via etherification and esterification reactions is considered to be a beneficial alternative for glycerol utilization, because these value-added chemicals have potential uses in versatile industrial applications [3,4]. In particular, acetylation of bio-glycerol with acetic acid into glycerol-esters is of interest, because the mono-, di-, and triacetylated glycerol products, namely mono-, di-, and triacetin, have various uses in cryogenics, and as raw materials for biodegradable polyesters, cosmetics, and fuel additives [3,5]. Special interest has been focused on di- and triacetin because of their potential for vast quantity utilization as valuable biodiesel and petro fuel additives [6–8].

Glycerol acetylation with acetic acid can be conducted at relatively mild temperatures conventionally by using mineral acids [9]; however, the homogeneous acid catalysts are toxic, corrosive, and difficult to remove, so they impose significant drawbacks on the process and environmental aspects. Heterogeneous acid catalysts can be advantageous alternatives for surpassing such critical limitations, and have been investigated extensively in recent studies. Melero et al. studied the catalytic properties of the alkylated

* Corresponding author. Tel.: +82 2 6490 2371; fax: +82 2 6490 2364.
E-mail address: dolee@uos.ac.kr (D. Lee).

0926-3373/$ – see front matter © 2013 Elsevier B.V. All rights reserved.
http://dx.doi.org/10.1016/j.apcatb.2013.11.008

sulfonic acids (propyl-, arene-, and perfluoro-sulfonic acid) functionalized siliceous mesoporous SBA-15, and reported that the formation rates of di- and triacetin increased as the acid strength of the sulfonic acid groups increased, while an enhanced mass transport property was concomitantly offered by mesoporous SBA-15 support [10]. The resin type solid acids, such as commercial Amberlyst and Dowex catalysts consisting of ion-exchanged sulfonic acid groups in the structures, are also extensively applied for the reactions [11–13]. The Keggin type heteropolyacids (HPAs) of molybdo- and tungstophosphoric acids have been investigated as immobilized forms onto high surface area silica [14], zeolites [15], SBA-15 [16], activated carbon [17], niobia [18], and Cs-containing zirconia [19] to provide enhancements in the active surface area and stability of the HPA moieties. Several protonic form zeolites such as HZSM-5 and HUSY [20,21], as well as acidic metal oxides such as niobia [20] and zirconia based multi-metal oxides [22], have also been of interest for the reactions. Various sulfated solid acids that are obtained by impregnation of sulfuric acid on activated carbon [23,24], ZrO_2 [25], and CeO_2–ZrO_2 and CeO_2–Al_2O_3 [26] followed by oxidative heat treatments, have been investigated for glycerol acetylation.

Although there have been many studies on various solid acid catalysts for glycerol acetylation, comparative studies that comprehensively assess the catalytic properties of different types of solid acids at similar and controlled reaction conditions based firmly on the types of acid sites, surface acidity, and acid strength of the catalysts has been limited. Herein, we have investigated glycerol acetylation with acetic acid on various solid acids: silica–alumina, HUSY, dodecamolybdophosphoric acids supported on Nb_2O_5 (HPMo/Nb_2O_5) and mesoporous SBA-15 (HPMo/SBA-15), Amberlyst-15, sulfated ceria–zirconia (SCZ), propylsulfonic acid functionalized SBA-15 ($PrSO_3H$-SBA-15), and sulfonic acid functionalized SBA-15 (SO_3H-SBA-15) and microcrystalline cellulose (SO_3H-Cell) catalysts. The intrinsic catalytic properties based on glycerol conversion turnover rate and selectivity toward mono-, di-, and triacetin products on these catalysts were extensively compared and characterized under the same reaction condition, and the results were correlated with the physicochemical properties of the catalysts in details.

2. Experimental

2.1. Catalysts synthesis

Silica–alumina (Aldrich, Si/Al atomic ratio = 6.2) and HUSY (Alfa, Si/Al = 160) were purchased as fine powders and used without further modifications. Amberlyst-15 (Rohm & Haas), which was supplied as beads (surface area = 53 $m^2\,g^{-1}$, average diameter = 0.74 mm), was crushed and sieved into fine powders (125–180 μm) to eliminate the effects of internal mass transfer hindrance in the reaction rate assessment. Mesoporous SBA-15 was prepared according to the procedure reported by Zhao et al. [27]. Dodecamolybdophosphoric acid ($H_3PMo_{12}O_{40}$, referred to as HPMo) immobilized onto SBA-15 (HPMo/SBA-15) was prepared by impregnation with a loading amount of HPMo at 25 wt%. Briefly, 1 g of $H_3PMo_{12}O_{40}{\cdot}xH_2O$ (Alfa) was dissolved in 30 ml of methanol (Samchun, HPLC grade), and 3 g of SBA-15 was added at room temperature. The mixture was stirred for 7 h, dried at 343 K to evaporate the solvent, and finally calcined at 623 K for 2 h (ramp = 1 K min^{-1}) [28]. The HPMo impregnated Nb_2O_5 (HPMo/Nb_2O_5) was prepared using a similar procedure with the loading amount of HPMo on the Nb_2O_5 (Junsei Chemical) also at 25 wt%. The resultant was dried at 393 K for 12 h and calcined at 573 K for 2 h [18].

Sulfonic acid functionalized SBA-15 (SO_3H-SBA-15) was prepared by immobilization of sulfonic acid groups on SBA-15 by using chlorosulfonic acid ($ClSO_3H$, Aldrich, 99%) as a precursor. 5.0 g of SBA-15 was dispersed in 40 ml of n-hexane (Aldrich, HPLC grade) with vigorous stirring in a beaker placed in an ice bath, and 9.0 mmol of chlorosulfonic acid was slowly added in a dropwise manner for 2 h. The resultant was filtered, washed with acetonitrile (Aldrich, 99.9%), and dried in air at room temperature for 12 h. Sulfonic acid grafted cellulose catalyst (SO_3H-Cell) was prepared using the same procedure that was used for the SO_3H-SBA-15. The cellulose used for the support was microcrystalline powders (Alfa, particle size < 220 μm), and the final form of SO_3H-Cell was obtained after drying the sample at room temperature for 12 h [29]. Propylsulfonic acid functionalized SBA-15 ($PrSO_3H$-SBA-15) was prepared according to the method reported by Melero et al. [30]. An aqueous solution containing 4 g of Pluronic P123, 125 g of 1.9 M HCl, and 7.7 g of TEOS was prepared at 313 K, and 0.8 g of 3-mercaptopropyltrimethoxysilane (MPTMS, Alfa, 95%) and 1.3 g of hydrogen peroxide (Alfa, 29–32%) were added subsequently. The resultant was stirred for an additional 20 h, and the hydrothermal synthesis was conducted in a static condition at 373 K for 24 h. The resultant was centrifuged, washed with a copious amount of ethanol under reflux for 24 h, and dried at 373 K for 12 h.

Sulfated CeO_2–ZrO_2 catalyst (SCZ) was prepared using the procedure reported by Reddy et al. [26]. The CeO_2–ZrO_2 support was obtained via co-precipitation of the mixed metal hydroxide from an aqueous mixture solution of zirconium nitrate hydrate ($ZrO(NO_3)_2{\cdot}xH_2O$, Alfa) and ammonium cerium nitrate ($(NH_4)_2Ce(NO_3)_6$, Deajung) at a Ce/Zr atomic ratio of 1.0 by adjusting the pH of the solution at 9.0 with an ammonium hydroxide titration solution (Alfa, 28 wt%) [31]. The precipitates were centrifuged, washed with distilled water, and dried in a convection oven at 383 K for 12 h. The resultant was impregnated with a 0.5 M H_2SO_4 aqueous solution (H_2SO_4/CeO_2–ZrO_2 hydroxide ratio = 5 ml g^{-1}) with stirring for 1 h at room temperature. The excess water was evaporated, and the resultant was dried at 393 K for 3 h and calcined at 873 K for 5 h (ramp = 10 K min^{-1}).

2.2. Catalyst characterization

Surface area and pore size distribution of the catalysts were characterized using N_2 adsorption–desorption isotherms obtained in a volumetric unit (Autosorb iQ, Quantachrome). The surface area was estimated applying Brunauer–Emmett–Teller (BET) theory. The micropore and mesopore size distributions were obtained with density functional theory (DFT) and Barrett–Joyner–Halenda (BJH) theory, respectively. Powder X-ray diffraction (XRD) patterns of the samples were obtained using monochromic Cu-K_α radiation operating at 40 kV and 40 mA with a step size of 0.05° and a scan rate of 1 step s^{-1} (AXS diffractometer D8, Bruker). The acidity on the catalysts was characterized by three different methods: neutralization titration [32] for Brönsted acidity, temperature programmed desorption (TPD) of ammonia (NH_3-TPD) for total acidity, and TPD of acetonitrile (CH_3CN-TPD) for Lewis acidity [33,34]. In the neutralization titration method, 0.05 g of catalyst powder was treated with 20 ml of a 1.0 M aqueous NaCl solution for 1 h at room temperature under sonication. After the centrifugal separation, the supernatant solution was titrated with a 0.01 M aqueous NaOH solution using phenolphthalein as the neutralization indicator. The TPD of NH_3 and CH_3CN was carried out in an automatic chemisorption unit (AutoChem 2910, Micromeritics). In the NH_3-TPD, the samples were pre-treated under a He flow (50 ml min^{-1}) at 423 K for 2 h followed by a diluted NH_3 flow (10 mol% NH_3/He-balance, 50 ml min^{-1}) at room temperature for 0.5 h, and finally held at 373 K under a He flow (50 ml min^{-1}) for 1 h to purge the weakly adsorbed NH_3 species. In the CH_3CN-TPD, the samples were pretreated at the same condition except that acetonitrile was introduced onto the sample by pulse injections using a micro-syringe under a He

carrier gas (50 ml min^{-1}) until the saturation was attained. The TPD characteristics of NH_3 and CH_3CN were obtained by raising the temperature of the samples from 373 K to 1173 K at various ramping rates between 5 and 30 K min^{-1}. The NH_3 desorption activation energy on the acid sites of the catalysts was characterized by applying the method reported by Redhead [35], which correlates desorption activation energy with temperature of the maximum desorption rate and heating rate according to Eq. (1):

$$\frac{E_d}{RT_p^2} = \frac{\nu}{\beta} \exp\left(\frac{-E_d}{RT_p}\right) \quad (1)$$

where E_d is activation energy of desorption, T_p is temperature at which desorption rate is the maximum, β is heating rate, and ν is pre-exponential factor of the desorption rate coefficient. The NH_3 desorption activation energy on Amberlyst-15, SO_3H-SBA-15, and SO_3H-Cell could not be obtained using this method due to their thermal instability at elevated temperatures. Therefore, the NH_3 desorption energy barrier on these catalysts was estimated from the experimental heat of adsorption values reported in the literature and density functional theory (DFT) calculation (B3LYP/6-31G(2d,p)) using Gaussian 09 software package.

2.3. Glycerol acetylation with acetic acid

Glycerol acetylation reaction was conducted at atmospheric pressure in a stirred batch reactor consisting of a three-necked glass flask (500 ml) equipped with a reflux condenser. The reactants used were mixtures of glycerol (Alfa, HPLC grade) and acetic acid (Alfa, Glacial 99.7%) at 1:6 and 1:9 molar ratios. In a typical experimental procedure, a reactant mixture containing 12.9 g of glycerol was added with 0.64 g of catalyst, and the temperature of the reactants was measured and isothermally maintained by placing the reactor in a PID-controlled electric heating mantle. The catalysts were dried at 373 K (313 K for Cell-SO_3H) in a convection oven for 12 h prior to utilization for the reactions. Sampling of the product mixture was carried out periodically during the reaction using a microsyringe, and the composition was analyzed by a flame ionization detector (FID)-equipped gas chromatograph (Agilent 7890, DB-5 column (30 m × 0.32 mm)). The stability of the catalysts was evaluated by performing consecutive batch runs under the same reaction conditions at 353 K; after each run, the catalysts were separated by filtration or centrifugation, washed with methanol (Amberlyst-15), ethanol (SiO_2–Al_2O_3, HUSY), ethanol and acetone ($PrSO_3H$-SBA-15), distilled water (HPMo/SBA-15, HPMo/Nb_2O_5), ethyl acetate (SCZ), or acetonitrile (SO_3H-SBA-15, SO_3H-Cell), and dried at 373 K for 12 h for the consecutive utilization. The glycerol acetylation reactions were conducted at different temperatures between 333 and 373 K, and the effects of reaction temperature were also investigated. The glycerol conversion turnover rate (h^{-1}) to each product was obtained by dividing the moles of glycerol that was converted to each product per unit catalyst amount and time (mol g_{cat}^{-1} h^{-1}) by the acidity of the catalyst (mol g_{cat}^{-1}). The kinetics assessment was conducted at a similar glycerol conversion of ~30% to eliminate the effects of varied reactant concentrations due to different activities of the catalysts.

3. Results and discussion

The BET surface areas of the SBA-15, Nb_2O_5, and CeO_2–ZrO_2 used for the supports of the catalysts were 845, 5, and 53 m^2 g^{-1}, respectively. All of the catalysts investigated in this work were utilized as fine powders in sizes below 220 μm. The Amberlyst-15 beads with average sizes of 0.7 mm were crushed into powders to eliminate the intraparticle mass transfer limitation; the glycerol conversion rate was approximately twofold higher on its powder form than on the beads (353 K, $C_2H_4O_2/C_3H_8O_3$ = 6), indicating that the large particle size of the initial bead form of the catalysts affected the rates by hindering internal mass transport. Variations in the stirring rate did not affect the glycerol conversion rates on all of the catalysts, suggesting that the liquid film mass transfer resistance was negligible.

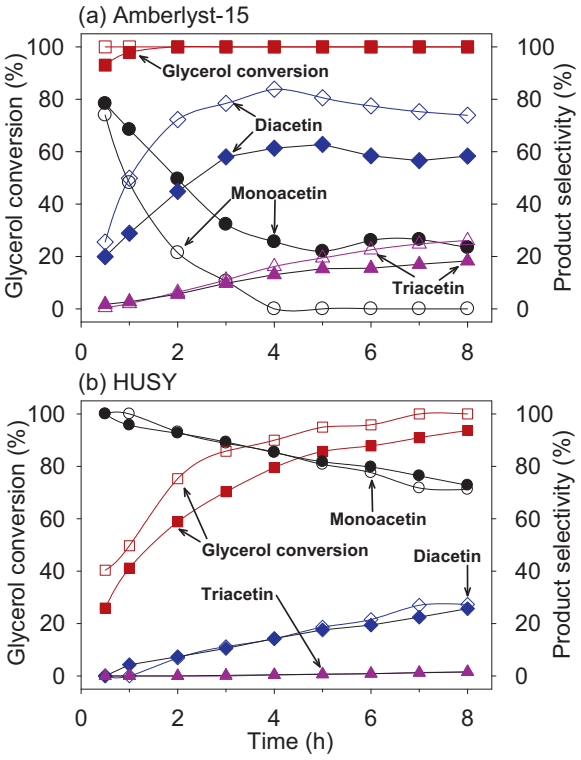

Fig. 1. Glycerol conversion on (a) Amberlyst-15 and (b) HUSY catalysts with respect to reaction time in a batch reactor at 353 K ($C_2H_4O_2/C_3H_8O_3$ molar ratio = 6 (closed symbols); $C_2H_4O_2/C_3H_8O_3$ = 9 (open symbols); catalyst loading = 5 wt% on the amount of glycerol reactant basis).

Fig. 1 shows the typical glycerol conversion and product selectivity with respect to reaction time for glycerol acetylation on (a) Amberlyst-15 and (b) HUSY at 353 K for two different $C_2H_4O_2/C_3H_8O_3$ reactant molar ratios of 6 and 9, respectively. The fast glycerol conversion and notably high monoacetin selectivity in the early stage of the reaction on these catalysts indicated that the formation of monoacetin was substantially easier than its further acetylation into di- and triacetin. The results reflect the thermodynamic characteristics of the reactions, in which Gibb's free energy for formation of 1-monoacetin (19.2 kJ mol^{-1}), which was obtained by DFT calculation (B3LYP/6-31G(d,p)), is considerably lower than those of 1,3-diacetin (37.0 kJ mol^{-1}) and triacetin (92.5 kJ mol^{-1}) [36]. The reactant molar composition affected the conversion rate and product selectivity toward di- and triacetin in favor of an elevated $C_2H_4O_2/C_3H_8O_3$ ratio. However, the enhancement in their equilibrium conversion was marginal only in several percents, even for a sizeable increase in the $C_2H_4O_2/C_3H_8O_3$ ratio from 6 to 9. Table 1 displays the glycerol conversion and product selectivity on various solid acid catalysts obtained at 353 K for 8 h of the batch reaction under the same weight amount of catalyst loading (5 wt% on the basis of the glycerol feed). Mono-, di-, and triacetin were exclusively produced on these catalysts, and the formation of other hydrocarbons or oxygenated hydrocarbons was not observed. The results show that glycerol conversions on these catalysts were high with values near 100% due to facile glycerol conversion to monoacetin, whereas the selectivity toward

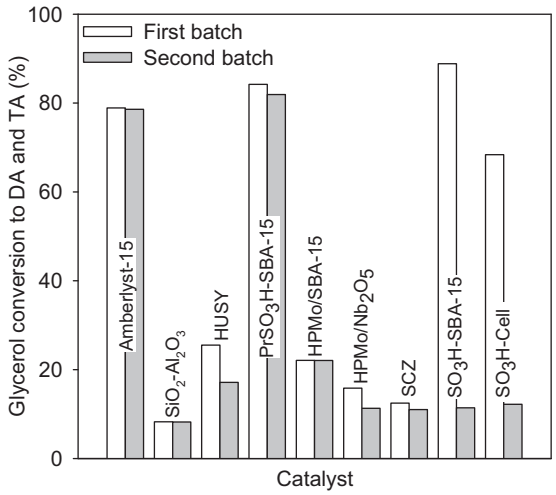

Fig. 2. Glycerol conversion to combined diacetin (DA) and triacetin (TA) products at 353 K. Two consecutive batch runs were displayed at the same reaction condition for 8 h (reactants = glycerol 12.9 g, $C_2H_4O_2/C_3H_8O_3$ molar ratio = 6; catalyst loading = 5 wt% on the amount of glycerol reactant feed basis).

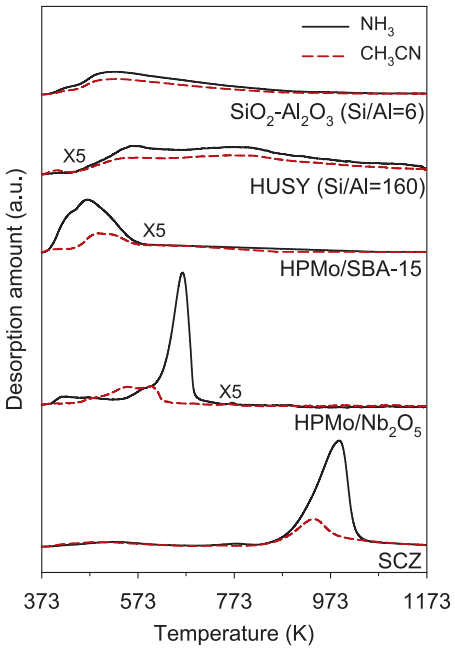

Fig. 3. Temperature programmed desorption (TPD) characteristics of NH_3 and CH_3CN adsorbed on various solid acid catalysts (ramping rate = 10 K min^{-1}).

di- and triacetin exhibited a considerable difference reflecting varied activities of the catalysts for these highly acetylated products. Therefore, catalytic properties of these solid acids were assessed based on the conversion rate toward di- and triacetin. Particularly higher glycerol conversion and selectivity toward di- and triacetin was noticeable on Amberlyst-15, $PrSO_3H$-SBA-15, SO_3H-SBA-15, and SO_3H-Cell. Fig. 2 displays the stability of the catalysts that was investigated by conducting consecutive reaction batches with the utilized catalysts under the same reaction conditions. It turned out that SO_3H-SBA-15 and SO_3H-Cell deactivated almost completely for two consecutive batch runs, different from the other solid acids that were relatively stable under the repeated utilization. The main reason for the deactivation of SO_3H-SBA-15 and SO_3H-Cell was identified as a substantial loss in their acidity; the Brönsted acidity on SO_3H-SBA-15 decreased from 0.80 to 0.36 mmol H^+ $g_{cat}{}^{-1}$, and that on SO_3H-Cell decreased from 1.30 to 0.15 mmol H^+ $g_{cat}{}^{-1}$ after the first batch run. These significant acidity loss occurred by hydrolysis of the sulfonic acid group that was grafted onto the supports by a single ether type atomic linkage. In the presence of the H_2O glycerol acetylation byproduct, these sulfonic acid groups can be easily removed from the support into molecular H_2SO_4, as evidenced from the complete acidity loss on the catalysts after boiling in distilled water at 373 K for 12 h. Apparently, the high glycerol conversion in the first reaction batch on these catalysts was mainly due to occurrence of the homogeneous reactions in the presence of molecular H_2SO_4 that was removed from the supports. Potential applications of the similar cellulose sulfonic acid catalysts were suggested in previous studies emphasizing the benefits of utilizing renewable resources, and they were applied to condensation type reactions involving hydrolysis environments [37,38]. It appears that stability of the grafted sulfonic acid groups and cellulose matrix on this type of catalysts should be carefully assessed to determine whether the reactions may degrade the integrity of the catalyst structures.

Fig. 3 shows NH_3-TPD and CH_3CN-TPD patterns on SiO_2–Al_2O_3, HUSY, HPMo/SBA-15, HPMo/Nb_2O_5, and SCZ catalysts. The total and Lewis acidity on these samples were estimated from the NH_3 and CH_3CN desorption amount, respectively. Decomposition of organic constituents in Amberlyst-15, $PrSO_3H$-SBA-15, SO_3H-SBA-15, and SO_3H-Cell can occur at elevated temperatures [39–41], therefore Brönsted acidity on these catalysts was obtained by the neutralization titration. The method specifically quantifies Brönsted acid sites and was also complementarily applied on SiO_2–Al_2O_3, HUSY, HPMo/SBA-15, HPMo/Nb_2O_5, and SCZ. Table 2 summarizes the Brönsted, Lewis, and total acidity on the samples obtained by the TPD and titration methods. The Brönsted acidity obtained by the neutralization titration on Amberlyst-15 showed an excellent agreement with the value provided by the supplier (4.7 mmol g^{-1}) reflecting validity of the method. In addition, the Lewis acidity on SiO_2–Al_2O_3, HUSY, and SCZ catalysts that were characterized by CH_3CN-TPD also showed good agreements with

Table 1
Glycerol conversion and product selectivity on various solid acid catalysts at 353 K.

Catalyst	Glycerol conversion (%)	Glycerol conversion to DA and TA (%)	Product selectivity (%)		
			MA	DA	TA
Amberlyst-15	100	79	21.1	63.8	15.1
Silica–alumina	71	8	88.5	11.2	0.3
HUSY	94	26	72.7	25.7	1.6
$PrSO_3H$-SBA15	100	84	15.8	64.6	19.6
HPMo/SBA15	96	22	77.1	22.0	0.9
HPMo/Nb_2O_5	87	16	81.8	17.5	0.7
SCZ	81	12	84.7	14.8	0.5
SO_3H-SBA15	100	89	11.1	61.9	27.0
SO_3H-Cell	100	68	31.6	55.0	13.4

The results were obtained after 8 h of glycerol acetylation ($C_2H_4O_2/C_3H_8O_3$ molar ratio = 6, catalyst loading = 5 wt% based on the amount of glycerol feed, MA = monoacetin, DA = diacetin, TA = triacetin).

Table 2
Properties of the solid acid catalysts.

Catalyst	Surface area ($m^2\ g_{cat}^{-1}$)	Average pore size (nm)	Brönsted acidity (mmol g_{cat}^{-1})	Lewis acidity (mmol g_{cat}^{-1})	Total acidity (mmol g_{cat}^{-1})	NH_3 desorption activation energy (kJ mol^{-1})
Amberlyst-15	53	30	4.9	–	4.9	125[c]
SiO_2–Al_2O_3	527	5.8	0.8	3.1 (2.4[b])	3.2	124
HUSY	790	0.9	0.3	0.6 (0.6[b])	0.9	150
$PrSO_3H$-SBA-15	701	7.0	1.2	–	1.2	143[c]
HPMo/SBA-15	607	5.4	0.5[a]	0.1	0.6	167
HPMo/Nb_2O_5	7	2.9	0.6[a]	0.1	0.7	239
SCZ	19	4.3	2.9	1.3 (1.2[b])	4.1	264
SO_3H-SBA-15	515	4.6	0.8	–	0.8	–
SO_3H-Cell	–	–	1.3	–	1.3	–

[a] Obtained by subtracting the Lewis acidity from the total acidity.
[b] Obtained by subtracting the Brönsted acidity from the total acidity.
[c] Estimated by the correlation using experimental adsorption enthalpy results.

the values obtained by subtracting the Brönsted acidity from the total acidity obtained by the titration and NH_3-TPD, respectively. On SiO_2–Al_2O_3, a broad NH_3-TPD pattern appeared with desorption maximum at 428 and 522 K, where the small low temperate peak at 428 K was attributed to the desorption of the weakly physisorbed NH_3 species. The broad NH_3 desorption pattern that developed over the elevated temperatures with a maximum at 522 K indicated that acid sites of various acid strengths presented over the catalyst surface [42]. On HUSY, two distinct NH_3 desorption peaks appeared at 563 and 769 K. The relatively intense low temperature peak at 563 K suggested that a considerable amount of NH_3 species resided on the inner cage of HUSY without strong stoichiometric interactions with the surface acid sites [43,44]. The intense and broad peak that was developed with a maximum at 769 K was assigned to desorption of the stoichiometrically adsorbed NH_3 species over the surface acid sites. The desorption temperature of these species was higher on HUSY (Si/Al = 160) than on SiO_2–Al_2O_3 (Si/Al = 6.2), which was reasonable considering that the higher Si/Al atomic ratio on HUSY would give rise to a higher acid strength. Desorption of NH_3 on HPMo/SBA-15 and HPMo/Nb_2O_5 occurred at different temperatures, suggesting substantial effects of the supports on the properties of the impregnated HPMo moieties. It has been reported that silica supports induce thermal decomposition of HPMo into β-MoO_3 species at temperatures above 523 K [45]. The surface dispersion of impregnated HPMo moieties was higher on SBA-15 (surface area = 845 $m^2\ g^{-1}$) than on Nb_2O_5 (5 $m^2\ g^{-1}$), and this would increase the interactions of the HPMo with the siliceous surface, thereby facilitating decomposition of Keggin units upon calcination at elevated temperatures. Decomposition of the structure was evidenced by XRD results, in which the crystallized HPMo moieties on HPMo/SBA-15 completely disappeared after the calcination treatment at 623 K, while the characteristic diffraction feature remained somewhat on HPMo/Nb_2O_5. Therefore, it is reasonable to assign that the peak developed at 468 K on HPMo/SBA-15 was due to NH_3 desorption from the decomposed HPMo surface moieties, while the peak observed at 667 K on HPMo/Nb_2O_5 was due to desorption from slightly disordered HPMo crystallites. On SCZ catalyst, the desorption of NH_3 occurred at significantly higher temperatures showing a maximum at 990 K, which indicated the strong acid strength of the surface acid sites that formed on the sulfated ceria–zirconia surface. The result agree well with the previous findings reported in the literature that explain that sulfated species on metal oxides can attract electrons generating Lewis acid centers, which also enhance Brönsted acid strength of the acidic hydroxyl groups on the catalyst surface [46,47].

In order to take the different acidities of various solid acid catalysts into account in the assessment of their catalytic properties, the reactions were carried out at the same number of acid sites loading (2.0 mmol) by adjusting the amounts of catalysts that were utilized for the reaction. Fig. 4 displays the glycerol conversion and product selectivity obtained for 8 h of the batch reaction at (a) 353 and (b) 373 K, respectively. At both temperatures, the catalysts generally showed high glycerol conversions, while the product selectivity was considerably different among the catalysts. At 353 K, the glycerol conversion on Amberlyst-15, $PrSO_3H$-SBA-15, and HUSY reached 100%, and the selectivity of mono-, di-, and triacetin products were nearly equilibrated. On SiO_2–Al_2O_3, HPMo/SBA-15, HPMo/Nb_2O_5, and SCZ catalysts, the glycerol conversions were moderate and the major reaction product was monoacetin, while there was a little formation of triacetin. At 373 K, the product composition of most of the catalysts was equilibrated, except on SiO_2–Al_2O_3 and SCZ that showed relatively low di- and triacetin selectivity. The results also showed significant changes in the product selectivity on SiO_2–Al_2O_3, HPMo/SBA-15, HPMo/Nb_2O_5, and SCZ catalysts as the reaction temperature increased from 353 to 373 K, due to substantial enhancements in the formation rates for di- and triacetin. Fig. 5 displays the glycerol conversion turnover rate (h^{-1}) toward combined di- and triacetin products on the catalysts at (a) 353

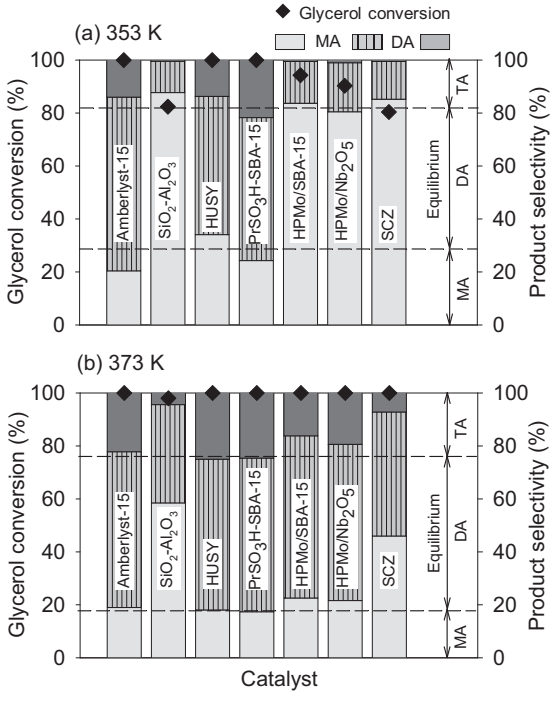

Fig. 4. Glycerol conversion and product selectivity on various solid acid catalysts for 8 h of glycerol acetylation at (a) 353 K and (b) 373 K. The results were obtained at the same number of acid sites loading condition (2.0 mmol, $C_2H_4O_2/C_3H_8O_3$ molar ratio = 6).

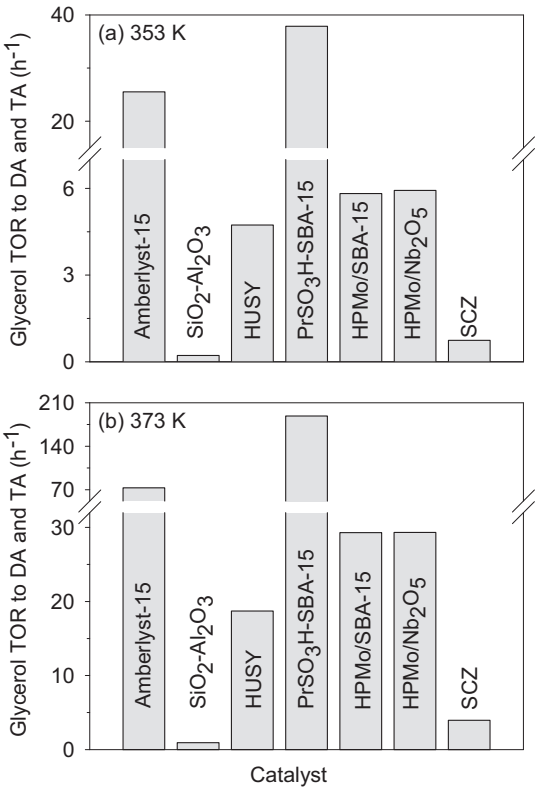

Fig. 5. Glycerol conversion turnover rate (TOR) to combined diacetin (DA) and triacetin (TA) products on various solid acid catalysts at (a) 353 and (b) 373 K. The TOR is compared at similar glycerol conversions (~30%) to DA and TA (reactants = glycerol 12.9 g, $C_2H_4O_2/C_3H_8O_3$ = 6, catalyst loading = 2 mmol of total acid sites).

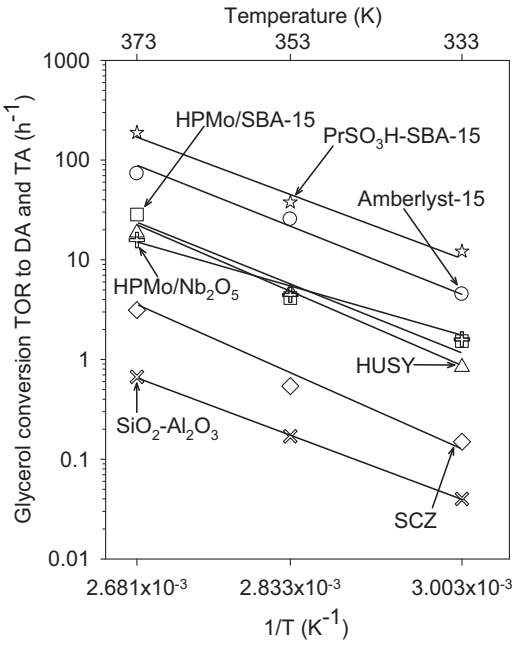

Fig. 6. Effects of reaction temperature on glycerol conversion turnover rate (TOR) to combined diacetin (DA) and triacetin (TA) products. TOR was compared at similar glycerol conversion levels (~30%) to combined DA and TA products (reactants = glycerol 12.9 g, $C_2H_4O_2/C_3H_8O_3$ = 6, catalyst loading = 2 mmol of total acid sites).

and (b) 373 K, respectively. These results were obtained at a similar glycerol conversion of ~30% in order to eliminate the effects of varied reactant concentrations during the reaction that can be imposed due to different activities of the catalysts. The results revealed that the glycerol conversion turnover rates on $PrSO_3H$-SBA-15 and Amberlyst-15 were substantially higher with the rates in order as follows: $PrSO_3H$-SBA-15 > Amberlyst-15 > HPMo/SBA-15 ≈ $HPMo/Nb_2O_5$ > HUSY > SCZ > SiO_2–Al_2O_3, both at 353 and 373 K. It is noteworthy that the glycerol reaction turnover to di- and triacetin was roughly two orders of magnitude higher on $PrSO_3H$-SBA-15 than on SCZ at 373 K, although the acid strength on SCZ was much greater than that on $PrSO_3H$-SBA-15. The temperature dependence of the glycerol conversion turnover rate to the combined di- and triacetin products on the catalysts was also investigated, and the results are presented as a function of temperature in Fig. 6. The results demonstrated that the glycerol conversion followed an Arrhenius type temperature dependence, with activation energies for the reactions between 60 and 80 kJ mol^{-1}. The linear regression fitting results were excellent with the coefficient of determination values, R^2, close to unity. Table 3 summarizes the pre-exponential factors and activation energies for the reactions on the catalysts. The results indicate that a relatively small temperature increase can lead to a considerable enhancement in the conversion rate toward di- and triacetin (k_{373}/K_{353} = 3–7), which is reflected in the large increase in the selectivity for these highly acetylated products at 373 K as shown in Fig. 4.

The effects of acid strength for the glycerol conversion turnover rate and product selectivity on the catalysts were examined in detail. The relative strength of the acid sites on the catalysts was estimated from NH_3 desorption activation energy obtained from NH_3-TPD by applying the method reported by Redhead as previously discussed (Eq. (1)). Fig. 7(a) displays the linear correlation fitting results for various NH_3 desorption maximum and heating rates obtained on the samples, in which the NH_3 desorption activation energy can be estimated from the slope of the fitting. The values on Amberlyst-15 and $PrSO_3H$-SBA-15 could not be obtained by NH_3-TPD due to their thermal instability at elevated temperatures. Therefore, the NH_3 desorption energy barrier on these catalysts were deduced from the experimental heat of adsorption values (ΔH_{ads}) that have been reported in literature: Amberlyst-15 = 110 kJ mol^{-1}, and $PrSO_3H$-SBA-15 = 128 kJ mol^{-1} [48–51]. The NH_3 adsorption energy (E_{ads}) on the catalysts was also determined by DFT calculations with B3LYP functional and 6-31G(2d,p) basis set using Gaussian 09 package. Fig. 7(b) displays the geometry-optimized minimum energy configurations of the NH_3-adsorbed-model-structure complexes for Amberlyst-15 (Benzene sulfonic acid, BSA) and $PrSO_3H$-SBA-15 ($PrSO_3H$-Si-$(OSiH_3)_3$) along with their zero-point energy corrected NH_3 adsorption energies. The theoretical calculation results revealed that NH_3 adsorption energies on the sulfonic acid functional groups of these two model structures were similar with approximate values of 60 kJ mol^{-1}. The NH_3 adsorption energy increased considerably by additional interactions with an adjacent sulfonic acid group as shown for

Table 3
Pre-exponential factor and activation energy for glycerol conversion turnover rate (TOR) to combined di- and triacetin products on the solid acid catalysts ($C_2H_4O_2/C_3H_8O$ = 6.0; catalyst loading = 2 mmol of total acid sites).

Catalyst	Pre-exponential factor × 10^{10} (h^{-1})	Activation energy (kJ mol^{-1})	Coefficient of determination (R^2)
Amberlyst-15	98	72.0	0.99
SiO_2–Al_2O_3	1.0	72.8	1.00
HUSY	321	80.1	1.00
$PrSO_3H$-SBA-15	124	70.4	0.98
HPMo/SBA-15	72	74.9	0.95
$HPMo/Nb_2O_5$	0.3	59.2	0.99
SCZ	25	78.2	0.98

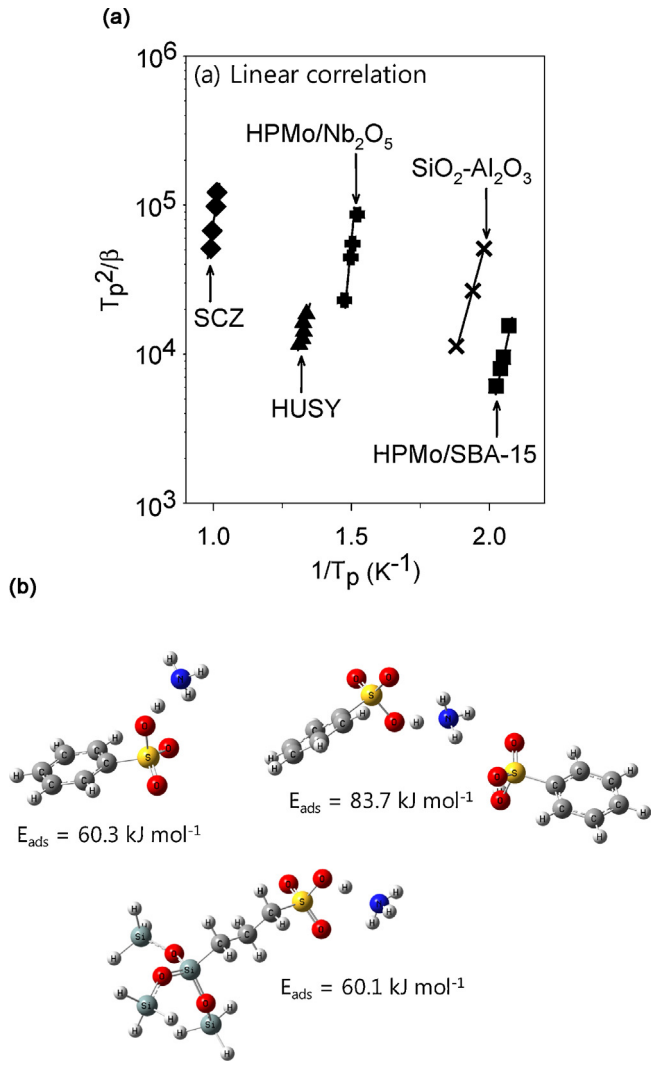

Fig. 7. (a) Linear correlation of T_p^2/β with respect to $1/T_p$ for NH_3-TPD on various solid acid catalysts (T_p = temperature of NH_3 desorption maximum, β = heating rate). (b) Geometry optimized minimum energy configurations of NH_3 adsorbed Amberlyst-15 (Benzene sulfonic acid) and $PrSO_3H$-SBA-15 ($PrSO_3H$-Si-$(OSiH_3)_3$) model structures and their zero point energy corrected NH_3 adsorption energies (E_{ads}).

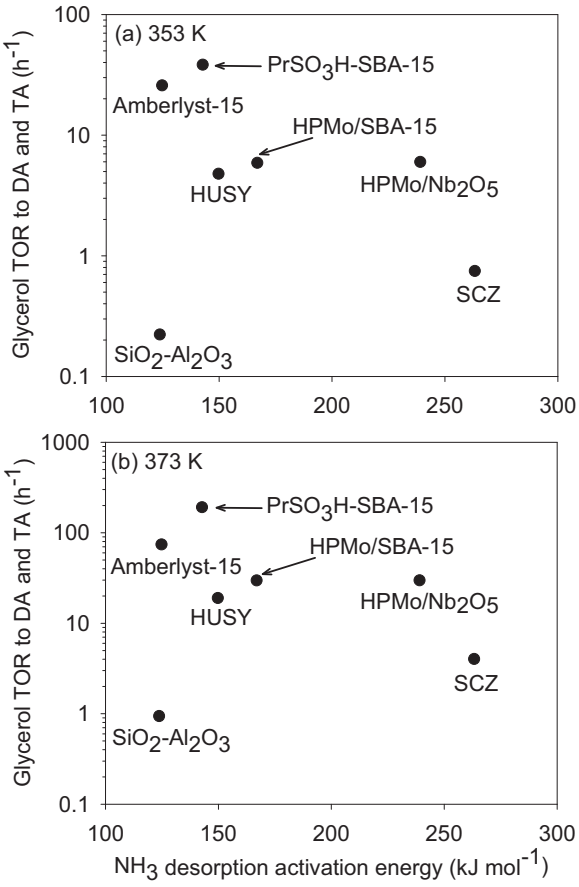

Fig. 8. Glycerol conversion turnover rate (TOR) to combined diacetin (DA) and triacetin (TA) on various solid acid catalysts with respect to the NH_3 desorption activation energy: (a) 353 K and (b) 373 K.

the NH_3-2BSA model complex (83.7 kJ mol^{-1}), and the results suggest that the spatial arrangements of the acidic functional groups on the catalysts can greatly affect the adsorption energy and configuration of the reactants on the surface. The desorption activation energy (E_d) of NH_3 can be treated as a summed value of the adsorption activation energy (E_0) and the heat of adsorption: $E_d = E_0 + \Delta H_{ads}$, where the adsorption activation energy would be much smaller than the heat of adsorption quantity. According to the linear correlation analysis by Hashimoto et al., the adsorption activation energies of NH_3 on various acidic zeolites were small with a similar value approximately of 15 kJ mol^{-1}, while the heat of NH_3 adsorption was considerably large with values between 80 and 150 kJ mol^{-1} [52,53]. Based on these previous findings, we estimated approximate values of the NH_3 desorption activation energy on Amberlyst-15 (125 kJ mol^{-1}) and $PrSO_3H$-SBA-15 (143 kJ mol^{-1}), and these were used for the analysis as will be discussed. Table 2 shows the NH_3 desorption activation energies on the catalysts. Fig. 8 displays the glycerol conversion turnover rates to combined di- and triacetin products on various solid acid catalysts with respect to the NH_3 desorption activation energy that reflect acid strength on the catalysts. Clearly, the results exhibited that the glycerol conversion turnover rate did not follow a proportional correlation with the acid strength on these catalysts neither at (a) 353 nor (b) 373 K. The substantially higher glycerol conversion turnover rates toward di- and triacetin were distinguishable on $PrSO_3H$-SBA-15 and Amberlyst-15, although their acid strengths were moderate and comparable to those on HPMo/SBA-15 and HUSY. Furthermore, the rates on $PrSO_3H$-SBA-15 and Amberlyst-15 were markedly higher than that on SCZ, while the acid strength on SCZ was substantially greater. These results were not due to the interplay of internal mass transfer hindrance. The catalysts were utilized as fine powders with sizes of several microns, except for Amberlyst-15 (125–180 μm) and SO_3H-Cell (<220 μm), in order to eliminate the intraparticle mass transfer limitation. In addition, the average pore size of the catalysts summarized in Table 2 did not indicate a dependence of the glycerol conversion turnover rate on the pore size of the catalysts, thereby suggesting that inner pore diffusion was not likely limiting the intrinsic rates. [The complete N_2 adsorption–desorption isotherms, pore size distributions, and pore volume analysis results are presented in supplementary information.] For example, the average pore size of SiO_2–Al_2O_3 and SCZ were 5.8 and 4.3 nm, respectively, with diameters that were approximately 2–6 times larger than those of HUSY (0.9 nm) and HPMo/Nb_2O_5 (2.9 nm); however, their catalytic activities for the reactions were significantly inferior. In addition, the glycerol conversion turnover rates on HPMo/SBA-15 and HUSY were similar, although their pore sizes differed significantly, supporting the fact that internal mass diffusion through these catalysts did not play

Table 4
Effect of H_2O for the glycerol conversion rates on various solid acid catalysts estimated by the initial rate difference measured with and without co-presence of H_2O in the reactants at 353 K ($C_2H_4O_2/C_3H_8O_3$ molar ratio = 6, catalyst loading = 5 wt% based on the amount of glycerol feed).

Catalyst	Glycerol conversion initial rate (mmol h^{-1})		Rate difference (%) $\left[\frac{r_2-r_1}{r_1} \times 100\right]$
	r_1 (without H_2O)	r_2 (5 wt% H_2O)	
Amberlyst-15	930	804	−14
SiO_2–Al_2O_3	33	24	−27
HUSY	71	72	1
$PrSO_3H$-SBA-15	1010	650	−36
HPMo/SBA-15	35	48	37
HPMo/Nb_2O_5	60	71	18
SCZ	31	34	10

a determining role for the apparent glycerol conversion rate and product selectivity.

The hydrophobic/hydrophilic nature of solid acid surface can affect the rate and product selectivity, therefore the effects of H_2O on the glycerol conversion rates were investigated by comparing the differences in the initial rates with and without the co-presence of H_2O (5.0 wt%) in the reactant feed. Table 4 summarizes the results. The adverse effects of H_2O on the rates were observed on $PrSO_3H$-SBA-15, SiO_2–Al_2O_3, and Amberlyst-15 with decreases in the rate, respectively, of 36, 27, and 14% due to the co-presence of H_2O in the reactants. Differently, the initial rates on HPMo/SBA-15, HPMo/Nb_2O_5, and SCZ increased, respectively, by 37, 18, and 10% in the co-presence of H_2O indicating inductive changes of the surface properties of these catalysts. The results suggest an occurrence of partial reconstruction of Keggin structure, as it has been reported that thermally decomposed HPMo moieties can rebuild to Keggin unit with exposure to water vapor [54]. HPMo/SBA-15 presented a greater initial rate increment than HPMo/Nb_2O_5 agreeing with its pristine morphological properties, because the quantitative reconstruction to Keggin structure would be greater on highly decomposed HPMo moieties on HPMo/SBA-15. However, it should be noted that this inductive effect was limited only in the first reaction batch and some extent of deactivation on these catalysts occurred during the consecutive batches due to leaching out of the HPMo constituents from the catalysts. [The complete results are shown in supplementary information.] The small increment in the glycerol conversion initial rate on SCZ was due to a slight additional formation of the acidic hydroxyl species on the dehydrated ceria–zirconia surface.

The results discussed above evidently demonstrated that the sulfonic acid functionalities presented on $PrSO_3H$-SBA-15 and Amberlyst-15 offered superior intrinsic catalytic activities for the glycerol acetylation reactions compared to the acid sites presented on SiO_2–Al_2O_3, HUSY, SCZ, and supported HPMo catalysts. An enhancement in the acid strength on solid acids can facilitate acetylation reactions of alcohols with acetic acid, and such favorable acid strength enhancement effects also held in this study when the analogous types of solid acids were compared ($HUSY > SiO_2$–Al_2O_3; $PrSO_3H$-SBA-15 > Amberlyst-15; HPMo/$Nb_2O_5 \geq$ HPMo/SBA-15). However, the comprehensive comparison results also indicated that configuration of the surface acid moieties may play a critical role in determining the catalytic properties of the solid acids with greater contributions than the acid strength. The inferior catalytic activity observed on SiO_2–Al_2O_3 and SCZ catalysts were not due to their relatively high Lewis acidity ratio on the total acid site constitution. This can be evidenced from the facts that the glycerol conversion turnover rates estimated by accounting only for the number of Brönsted acid sites on SiO_2–Al_2O_3 and SCZ are one to two orders of magnitude lower than those on the other catalysts. The reasons for the superior catalytic activity of the sulfonic acid functionalized $PrSO_3H$-SBA-15 and Amberlyst-15 are not clear at this point, but the results may reflect favorable mechanistic or energetic contributions on the immobilized sulfonic acid surface moieties for the reactions. The esterification reaction mechanism on homogeneous acid catalysts is well established on a protonated carboxylic acid intermediate with a rate determining nucleophilic substitution step by the hydroxyl group of an alcohol resulting in the water elimination. In the case of the reactions catalyzed by heterogeneous acid catalysts, vastly different mechanisms have been suggested depending on the catalysts and reactants. For acetylation of ethanol and n-butanol with acetic acid on activated carbon supported HPAs, Chu et al. proposed that the reaction proceeded by Langmuir–Hinshelwood (L–H) type mechanism for ethanol whereas it occurred by Eley–Rideal (E–R) type for n-butanol due to its preferential adsorption on the surface and steric effects [55]. Kirumakki et al. reported that the reactions of C_3–C_4 and benzyl alcohols on Hβ, HY, and HZSM-5 zeolites occurred by E–R type mechanism with protonated acetic acid species on the surface [56,57]. Diverse mechanisms also have been suggested on sulfuric acid functionalized solid resins. Altıokka et al. reported that isobutanol acetylation on Amberlite IR-120 proceeded by E–R type mechanism via reaction between surface isobutanol species and bulk phase acetic acid [58]. Conversely, Liu et al. proposed that esterification of n-butanol with propanoic acid on Amberlyst catalysts proceed via nucleophilic substitution of the protonated propanoic acid intermediate by n-butanol in the bulk [59]. Differently, Teo et al. reported L–H type mechanism for esterification of isoamyl alcohol with acetic acid on Purolite CT-175, suggesting that the rate-determining step was the reaction between the alcohol and acid species co-adsorbed on adjacent surface active centers [60]. These previous studies apparently indicate that subtle changes in the interaction properties between the surface acid sites and reactant species can significantly affect the kinetics of the reactions, beyond the extent that is contributed by the absolute acid strength of the acid sites. It is also clear that structural and spatial configuration of the surface acid moieties can interplay substantially on the interaction properties between the acid sites and reactants as shown by the DFT calculation results obtained in this work. In this respect, it is interesting to note that the sulfonic acid functionalized $PrSO_3H$-SBA-15 and Amberlyst-15, with a moderate Brönsted acid strength, showed markedly superior intrinsic activity for the reactions. Although more verification is required, it is reasonable to suggest based on the above facts that the structural configuration of sulfonic acid group and their spatial arrangements on the catalyst surface may favorably have interplayed give rising to the superior catalytic activity for the reactions. As a summary, the extensive comparison and characterization results on the catalytic properties of various solid acids for glycerol acetylation reactions obtained in this work indicated that sulfonic acid functionalized $PrSO_3H$-SBA-15 and Amberlyst-15 exhibit superior catalytic activity for the reactions. The results suggested that configuration of the surface acid moieties may play a substantial role in the intrinsic kinetics of glycerol acetylation, along with the acidity and acid strength properties on the solid acids.

4. Conclusions

The catalytic esterification of glycerol with acetic acid was studied on various types of solid acids: silica–alumina, HUSY, dodecamolybdophosphoric acids supported on Nb_2O_5 (HPMo/Nb_2O_5) and mesoporous SBA-15 (HPMo/SBA-15), Amberlyst-15, sulfated ceria–zirconia (SCZ), propylsulfonic acid functionalized SBA-15 ($PrSO_3H$-SBA-15), and sulfonic acid functionalized SBA-15 (SO_3H-SBA-15) and microcrystalline cellulose (SO_3H-Cell). The sulfonic acid functionalized $PrSO_3H$-SBA-15 and Amberlyst-15 catalysts

exhibited superior glycerol conversion turnover rates with high selectivity toward di- and triacetin products as compared to the other catalysts. The acid strength affected the rates, showing an increase in the intrinsic glycerol conversion turnover rate with an enhancement in the acid strength when the analogous type of solid acids was compared (HUSY > SiO_2–Al_2O_3; $PrSO_3H$-SBA-15 > Amberlyst-15; HPMo/Nb_2O_5 ≥ HPMo/SBA-15). The considerably higher glycerol conversion turnover rates observed on the sulfonic acid functionalized $PrSO_3H$-SBA-15 and Amberlyst-15 catalysts, in spite of their moderate Brönsted acid strength, suggested that the configuration and spatial arrangement of their surface acid moieties dominantly affected the catalytic properties for the reactions. The catalysts were stable during consecutive batch reactions, except of SO_3H-SBA-15 and SO_3H-Cell that showed significant deactivations due to substantial acidity loss by hydrolysis of the grafted SO_3H groups during the reactions.

Acknowledgements

The authors acknowledge support from the Korea Research Foundation (KRF 2011-0010095) and the human resources development program of the Korea Institute of Energy Technology Evaluation and Planning (KETEP) under a grant funded by the Korea Government Ministry of Trade, Industry, and Energy (2012-4010203260).

Appendix A. Supplementary data

Supplementary data associated with this article can be found, in the online version, at http://dx.doi.org/10.1016/j.apcatb.2013.11.008.

References

[1] A. Demirbas, Energy Convers. Manage. 50 (2009) 14–34.
[2] P. Kenkel, R. Holcomb, J. Menard, K. Jensen (Eds.), Integration of Agricultural and Energy Systems, Global Bioenergy Partnership, Atlanta, GA, 2008.
[3] N. Rahmat, A.Z. Abdullah, A.R. Mohamed, Renew. Sustain. Energy Rev. 14 (2010) 987–1000.
[4] A. Brandner, K. Lehnert, A. Bienholz, M. Lucas, P. Claus, Top. Catal. 52 (2009) 278–287.
[5] Y. Taguchi, A. Oishi, Y. Ikeda, K. Fujita, T. Masuda, JP Patent 298099 (2000).
[6] J.A. Melero, G. Vicente, G. Morales, M. Paniagua, J. Bustamante, Fuel 89 (2010) 2011–2018.
[7] E. Garcia, M. Laca, E. Perez, A. Garrido, J. Peinado, Energy Fuels 22 (2008) 4274–4280.
[8] R. Wessendorf, Derivates of Glycerol as Components of Fuels, vol. 48, Erdol Kohle, Erdgas, Pet., 1995, pp. 138–143.
[9] K. Maikhail, L.P. Van, US Patent 5777158 (1998).
[10] J.A. Melero, R. van Grieken, G. Morales, M. Paniagua, Energy Fuels 21 (2007) 1782–1791.
[11] L. Zhou, T.H. Nguyen, A.A. Adesina, Fuel Process. Technol. 104 (2012) 310–318.
[12] X. Liao, Y. Zhu, S.G. Wang, Y. Li, Fuel Process. Technol. 90 (2009) 988–993.
[13] I. Dosuna-Rodrigez, E.M. Gaigneaux, Catal. Today 195 (2012) 14–21.
[14] P. Ferreira, I.M. Fonseca, A.M. Ramos, J. Vital, J.E. Castanheiro, Appl. Catal. B 91 (2009) 416–422.
[15] P. Ferreira, I.M. Fonseca, A.M. Ramos, J. Vital, J.E. Castanheiro, Catal. Commun. 10 (2009) 481–484.
[16] M.S. Khayoon, B.H. Hameed, Appl. Catal. A: Gen. 433–434 (2012) 152–161.
[17] P. Ferreira, I.M. Fonseca, A.M. Ramos, J. Vital, J.E. Castanheiro, Catal. Commun. 12 (2011) 573–576.
[18] M. Balaraju, P. Nikhitha, K. Jagadeeswaraiah, K. Srilatha, P.S. Sai Prasad, N. Lingaiah, Fuel Process. Technol. 91 (2010) 249–253.
[19] K. Jagadeeswaraiah, M. Balaraju, P.S. Sai Prasad, N. Lingaiah, Appl. Catal. A: Gen. 386 (2010) 166–170.
[20] V.L.C. Gonçalves, B.P. Pinto, J.C. Silva, C.J.A. Mota, Catal. Today 133–135 (2008) 673–677.
[21] L. Zhou, E. Al-Zaini, A.A. Adesina, Fuel 103 (2012) 617–625.
[22] P.S. Reddy, P. Sudarsanam, G. Raju, B.M. Reddy, Catal. Commun. 11 (2010) 1224–1228.
[23] M.S. Khayoon, B.H. Hameed, Bioresour. Technol. 102 (2011) 9229–9235.
[24] J.A. Sánchez, D.L. Hernández, J.A. Moreno, F. Mondragón, J.J. Fernández, Appl. Catal. A: Gen. 405 (2011) 55–60.
[25] L. Wang, Q. Liu, M. Zhou, G. Xiao, J. Nat. Gas Chem. 21 (2012) 25–28.
[26] P.S. Reddy, P. Sudarsanam, G. Raju, B.M. Reddy, J. Ind. Eng. Chem. 18 (2012) 648–654.
[27] D. Zhao, Q. Huo, J. Feng, B.F. Chmelka, G.D. Stucky, J. Am. Chem. Soc. 120 (1998) 6024–6036.
[28] L. Lizama, T. Klimova, Appl. Catal. B 82 (2008) 139–150.
[29] J. Safari, S.H. Banitaba, S.D. Khalili, J. Mol. Catal. A: Chem. 335 (2011) 46–50.
[30] J.A. Melero, G.D. Stucky, R. Van Grieken, G. Morales, J. Mater. Chem. 12 (2002) 1664–1670.
[31] N. Guillén-Hurtado, A. Guillén-Hurtado, A. García-García, J. Mater. Sci. 47 (2012) 3204–3213.
[32] C. Zhang, Z. Fu, Y.C. Liu, B. Dai, Y. Zou, X. Gong, Y. Wang, X. Deng, H. Wu, Q. Xu, K.R. Steven, D. Yin, Green Chem. 14 (2012) 1928–1934.
[33] J. Penzien, T.E. Müller, J.A. Lercher, Microporous Mesoporous Mater. 48 (2001) 285–291.
[34] J.F. Haw, M.B. Hall, A.E. Alvarado-Swaisgood, E.J. Munson, Z. Lin, L.W. Beck, T. Howard, J. Am. Chem. Soc. 116 (1994) 7308–7318.
[35] P.A. Redhead, Vacuum 12 (1962) 203–211.
[36] X. Liao, Y. Zhu, S.G. Wang, H. Chen, Y. Li, Appl. Catal. B 94 (2010) 64–70.
[37] A. Shaabani, A. Maleki, Appl. Catal. A: Gen. 331 (2007) 149–151.
[38] A. Shaabani, A.H. Rezayan, M. Behnam, M. Heidary, C. R. Chim. 12 (2009) 1249–1252.
[39] V.V. Ordomsky, J.C. Schouten, J. van der Schaaf, T.A. Nijhuis, Chem. Eng. J. 207–208 (2012) 218–225.
[40] B. Sow, S. Hamoudi, M. Hassan Zahedi-Niaki, S. Kaliaguine, Microporous Mesoporous Mater. 79 (2005) 129–136.
[41] S.L. Quan, S.G. Kang, I.J. Chin, Cellulose 17 (2010) 223–230.
[42] N. Liu, S. Ding, Y. Cui, N. Xue, L. Peng, X. Guo, W. Ding, Chem. Eng. Res. Des. 91 (2013) 573–580.
[43] N. Katada, H. Igi, J.H. Kim, M. Niwa, J. Phys. Chem. B 101 (1997) 5969–5977.
[44] L. Rodríguez-González, E. Rodríguez-Castellón, A. Jiménez-López, U. Simon, Solid State Ionics 179 (2008) 1968–1973.
[45] A. Popa, V. Sasca, I. Holclajtner-Antunović, Microporous Mesoporous Mater. 156 (2012) 127–137.
[46] K. Arata, Adv. Catal. 37 (1990) 165–211.
[47] B.M. Reddy, M.K. Patil, P. Lakshmanan, J. Mol. Catal. A: Chem. 256 (2006) 290–294.
[48] P.F. Siril, A.D. Davision, J.K. Randhawa, D.R. Brown, J. Mol. Catal. A: Chem. 267 (2007) 72–78.
[49] S. Koujout, D.R. Brown, Thermochim. Acta 434 (2005) 158–164.
[50] P.F. Silril, D.R. Brown, J. Mol. Catal. A: Chem. 252 (2006) 125–131.
[51] M. Hart, G. Fuller, D.R. Brown, C. Park, M.A. Keane, J.A. Dale, C.M. Fougret, R.W. Cockman, Catal. Lett. 72 (2001) 135–139.
[52] T. Masuda, Y. Fujikata, S.R. Mukai, K. Hashimoto, Appl. Catal. A: Gen. 165 (1997) 57–72.
[53] T. Masuda, Y. Fujikata, H. Ikeda, S.I. Matsushita, K. Hashimoto, Appl. Catal. A: Gen. 162 (1997) 29–40.
[54] C. Rocchiccioli-Deltcheff, A. Aouissi, S. Launay, M. Fournier, J. Mol. Catal. A: Chem. 114 (1996) 331–342.
[55] W. Chu, X. Yang, X. Ye, Y. Wu, Appl. Catal. A: Gen. 145 (1996) 125–140.
[56] S.R. Kirumakki, N. Nagaraju, K.V.R. Chary, Appl. Catal. A: Gen. 299 (2006) 185–192.
[57] S.R. Kirumakki, N. Nagaraju, S. Narayanan, Appl. Catal. A: Gen. 273 (2004) 1–9.
[58] M.R. Altıokka, A. Cıtak, Appl. Catal. A: Gen. 239 (2003) 141–148.
[59] W.-T. Liu, C.-S. Tan, Ind. Eng. Chem. Res. 40 (2001) 3281–3286.
[60] H.T.R. Teo, B. Saha, J. Catal. 228 (2004) 174–182.